

Evaluation of heat and salt transports by mesoscale eddies in the Lofoten Basin

Tatyana Belonenko¹, Vadim Zinchenko¹, Svetlana Gordeeva^{1,2,3}, and Roshin P. Raj⁴

Received 28 January 2020; accepted 8 June 2020; published 4 December 2020.

The vertical structure of mesoscale eddies in the Lofoten Basin (LB) is investigated by combining satellite altimetry data and the Global Ocean Physics Reanalysis profiles (GLORYS12V1). We apply an automated eddy identification and tracking method to detect and track mesoscale eddies in the LB from altimeter data during the period 1993–2017. The three-dimensional structure of eddies detected is determined from GLORYS12V1 temperature and salinity profiles. A method based on the inferred three-dimensional structure of eddies and eddy trajectories is applied to estimate eddy heat and salt transports in a Lagrangian framework at each point of the track. Note that the study focuses on long-lived eddies (> 35 days) and all analyses are done separately for cyclonic and anticyclonic eddies. Further LB eddies are categorized into four groups based on the locations of eddy generation and dissipation. Our analysis focuses on the region of the quasi-permanent anticyclonic Lofoten Vortex (LV). The maximum in total heat transport associated with LB eddies (anticyclonic, 39.42×10^{13} W; cyclonic, 10.56×10^{13} W) is observed in the area outside the LV region. On the other hand, while the total salt transport by anticyclonic eddies (27.74×10^5 kg s⁻¹) is also the largest in the area outside the LV region, the maximum total salt transport by cyclonic eddies is found in the LV region (-12.32×10^5 kg s⁻¹). Furthermore, our analysis did not find any significant heat or salt transport into the LV region from the periphery of the Norwegian Current or its immediate neighborhood. The magnitude of heat and salt transports to the LV region from outside is estimated to be 0.9×10^{13} W and 1.18×10^5 kg s⁻¹, respectively. Annual averages are 3.6×10^{13} W for the heat and 7.2×10^3 kg s⁻¹ for the salt transport. These numbers estimate the cumulative transfer of heat and salt to the area of the LV from outside that effects on the annual winter regeneration of the LV. **KEYWORDS:** Lofoten Vortex; Lofoten Basin; Norwegian Sea; mesoscale eddies; altimetry; automatic identification algorithm; heat and salt transports; GLORYS12V1.

Citation: Belonenko, Tatyana, Vadim Zinchenko, Svetlana Gordeeva, and Roshin P. Raj (2020), Evaluation of heat and salt transports by mesoscale eddies in the Lofoten Basin, *Russ. J. Earth. Sci.*, 20, ES6011, doi:10.2205/2020ES000720.

¹St. Petersburg State University, St. Petersburg, Russia

²Russian State Hydrometeorological University, St. Petersburg, Russia

³Shirshov Institute of Oceanology RAS, Moscow, Russia

⁴Nansen Environmental and Remote Sensing Center and Bjerknes Center for climate Research, Bergen, N-5006, Norway

Introduction

Mesoscale variability in the World Ocean is manifested in the generation of mesoscale vortices as well as Rossby waves. Mesoscale eddies are vortices with scales ranging from the baroclinic Rossby radius of deformation to tens (hundreds) of kilometers. The main reason for their generation is the loss of stability by ocean currents. It consists of a

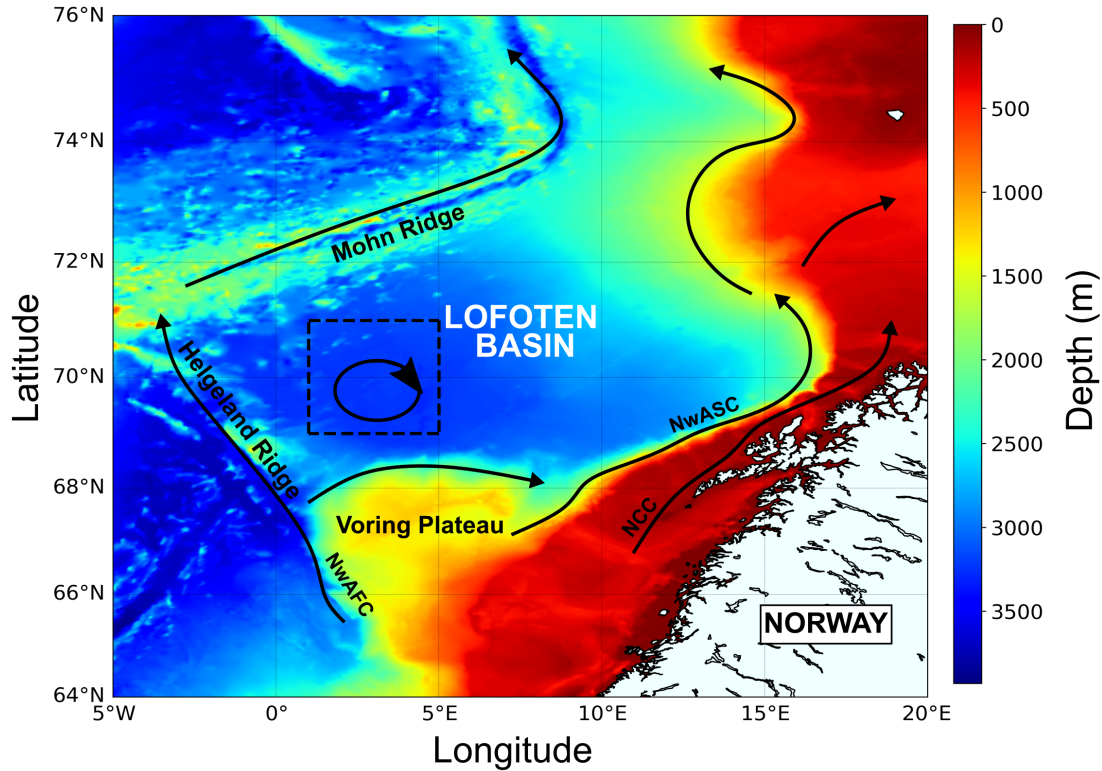


Figure 1. Bottom topography (color) and general circulation (arrows) of the study region. The black circle marks the Lofoten Vortex location. The black lines indicate the main currents. Abbreviations: NCC – Norwegian Coastal Current, NwASC – Norwegian Atlantic Slope Current, NwAFC – Norwegian Atlantic Frontal Current. The dotted black line shows the area of the Lofoten vortex (area 1).

sharp increase in the velocity of background flow or a change in its direction, resulting in barotropic or baroclinic instability of the flow (change of the density field with the distance) [Isachsen, 2015; Zhmur, 2011]. Another reason is external forcing such as fluctuating winds [Volkov and Fu, 2008]. In turn, these eddies interact with the mean flow and they transfer their kinetic energy back. These processes influence significantly the large-scale ocean circulation [Lozier, 1997; Morrow et al., 1994] and play an important role in the heat balance of boundary currents [Wunsch, 2009]. Advection of water by mesoscale eddies impact essentially to the total oceanic heat and salt transport [Belonenko et al., 2018; Dong et al., 2014; Morrow and Le Traon, 2012]. Heat and salt trapped by eddies change water properties in the ocean by advection of the eddies. Eventually, mesoscale eddies influence greatly the biology of the ocean and biological productivity of water, too [see, e.g., Belonenko et al., 2011;

Chelton et al., 2011; Gaube et al., 2015; Kubryakov et al., 2016; Raj et al., 2016].

The Lofoten Basin (LB) is a topographic depression of about 3250 m depth, bounded by the Voring Plateau in the south, Mohn's Ridge in the northwest, and the Eurasian continental shelf in the east (Figure 1). This makes the LB quite a separate topographic formation with specific features of large-scale oceanic circulation. The LB is bordered by two main branches of the Norwegian Atlantic Current (NwAC), the Norwegian Atlantic Slope Current (NwASC), and the Norwegian Atlantic Frontal Current (NwAFC). The NwASC flows along the continental slope while the NwAFC follows the Mohn Ridge along the 2000–2500 m isobaths. The NwASC is about two times stronger than the NwAFC with values of speed and volume transport twice as big as those of the NwAFC [e.g. Mork and Skagseth, 2010]. The NwASC also has a prominent seasonal cycle that has been linked

to wind forcing [*Jakobsen et al., 2003; Mork and Skagseth, 2010; Skagseth et al., 2015*].

The LB is the deepest and broadest reservoir of Atlantic water and thereby of the ocean heat content in the Nordic Seas [*Bjork et al., 2001*]. Furthermore, the LB is the most eddy-rich region of the Nordic Seas [e.g., *Bloshkina and Ivanov, 2016; Jakobsen et al., 2003; Poulain et al., 1996*], where large ocean-atmosphere interactions occur [*Rossby et al., 2009b*]. Being a transit area for the warm and saline Atlantic water on its way to the Arctic Ocean, the LB plays an important role in sustaining the Meridional Overturning Circulation, since this is a region where the Atlantic water loses its heat to the atmosphere and mixes with the surrounding water [*Orvik, 2004*].

An important feature of the LB is the high-intense synoptic-scale variability of mesoscale eddies. The region of the LB, well recognized as an area of energetic mesoscale activity, also has substantial heat loss to the atmosphere [*Rossby et al., 2009a; Richards and Straneo, 2015; Raj et al., 2016; Yu et al., 2017*]. Similar to other parts of the World Ocean, both anticyclonic (ACEs) and cyclonic (CEs) eddies characterize the mesoscale eddy activity of the Lofoten Basin [e.g., *Kohl, 2007; Raj et al., 2015*]. The most remarkable dynamical phenomenon in the center of the LB is a quasi-permanent anticyclonic eddy known as the Lofoten Vortex (LV), represented by a convective lens of warm and saline water in the 300–1000 m depth interval with a horizontal scale on the order of 100 km [*Alexeev et al., 1991; Bashmachnikov et al., 2017; Fedorov et al., 2019; Ivanov and Korabely, 1995*] discovered during Russian hydrological surveys in 1970s–1980s. Since then, several studies have confirmed the existence of the LV using in situ research [*Alexeev et al., 2016; Koszalka et al., 2011; Rossby et al., 2009a; Soiland and Rossby, 2013*], satellite altimetry [*Raj et al., 2015, 2016*], and ocean model data [*Kohl, 2007; Volkov et al., 2015*]. Recent observations and modeling studies have provided evidence that eddies reaching the center of the LB are the main mechanism maintaining the permanent LV [*Kohl, 2007; Raj et al., 2015; Volkov et al., 2015*].

In this paper, we use satellite altimeter data to track individual eddies of the LB. To analyze temperature and salinity (T/S) anomalies inside eddies in the LB, we apply the co-located method which

allows finding appropriate vertical T/S profiles for eddies detected. The main objective of this work is to estimate the amount of heat and salt transports by long-lived mesoscale eddies in different areas of the LB, and especially from the periphery of the LB to its center where the LV resides. We analyze T/S anomalies relative to the background conditions along the eddy tracks, and besides, we detect places of eddy generation and dissipation in the LB. The study tries to address the main question: what is the respective role of mesoscale eddies on the volume, heat and salt transports in the LB?

Data

We use high-resolution ($0.25^\circ \times 0.25^\circ$ grid) sea level anomalies (SLA) for the 25 years (1993–2017) to study the mesoscale eddies in the LB. The AVISO gridded altimetry data is a product (ID is SEALEVEL_GLO_PHY_L4_REP_OBSERVATION_NS_008_047) obtained from the Copernicus Marine Services. This product is processed by the SL-TAC multimission altimeter data processing system and includes data from all altimeter missions: Jason-3, Sentinel-3A, HY-2A, Saral/AltiKa, Cryosat-2, Jason-2, Jason-1, T/P, ENVISAT, GFO, ERS1/2. It provides a consistent and homogeneous catalog of products for varied applications, both for near real-time applications and offline studies.

To study the vertical structure of eddies we use Global Ocean Physics Reanalysis. The GLORYS12 V1 product is available at the Copernicus Marine Services. It is the CMEMS global ocean eddy-resolving ($1/12^\circ$ horizontal resolution and 50 vertical levels) reanalysis covering the period of 1993–2017 with a reduced-order Kalman filter. GLORYS12V1 uses assimilations the along-track altimeter data with high-resolution (7 km), as well as satellite Sea Surface Temperature, Sea Ice Concentration and in situ temperature and salinity vertical profiles. The GLORYS12V1 product is based on the NEMO model platform and it uses the ECMWF ERA-Interim reanalysis at the surface. A 3D-VAR scheme provides a necessary correction to the slow-evolving large-scale biases in temperature and salinity. This product includes daily and monthly data.

Methods

The open-source code for automatic identification and tracking of eddies developed by *Faghmous et al.* [2015] obtained from <https://github.com/jfaghm/OceanEddies>, is applied on the SLA data for the detection and tracking of mesoscale eddies in the LB. The eddy detection algorithm, which identifies eddies along closed contours is detailed as follows. It is based on the assumption that there can be only one extremum in the contour of the eddy (minimum or maximum, depending on the type of the eddy). The extremum is defined as a grid cell where the value of data is smaller (for the minimum) or greater (for the maximum) than the other values in the specified vicinity of the point. The choice of the vicinity is made on a uniform grid, to which the initial data have been previously interpolated. A contour of the eddy is determined by step-by-step iterations with an increase or decrease in the critical SLA value within the contour with a step chosen by the user until the assumption of a single extremum within the contour is violated, and after that, the eddy can be indicated by the contour formed at the previous iteration. This method may lead to a reassessment of the size of the vortex but the error is not so significant with the correct choice of the iterative step. The algorithm identifies cyclonic and anticyclonic eddies separately, calculating for each of them the following parameters: radius, amplitude (elevation or lowering of sea level at the extremum), and the area inside the contour and an azimuth velocity.

After identifying eddies from SLA maps, a procedure for tracking eddies moving in the basin is applied. We apply the eddy identification algorithm by *Faghmous et al.* [2015] to the maps of sea level anomalies (SLA) available on the link <http://marine.copernicus.eu>. To limit the search space, the algorithm estimates the probable velocity of the eddy moving, considering it as a phase velocity of a long (non-dispersive) Rossby baroclinic wave in the long-wave approximation, taking into account the Rossby baroclinic radius [*Chelton et al.*, 1998]. To give a physical meaning to binding eddy procedure at timesteps t and $t+1$, their external parameters are compared, i.e. the size and the amplitude. Eddies are connected if the ratios of the compared parameters during consecutive timesteps are within the range from 0.25 to 2.75. Note that

Table 1. Spatially Averaged Mean Parameters of Mesoscale Eddies in the LB

Parameter	Type of the eddies	Mean
Amplitude, cm	CEs	5.2
	ACEs	6.2
Radius, km	CEs	55.0
	ACEs	55.1
Azimuthal velocity, cm/s	CEs	28.2
	ACEs	32.3
Moving speed, km/day	CEs	4.0
	ACEs	4.0
Lifetime, days	CEs	46.4
	ACEs	50.8

it is probable that sometimes the eddies may temporarily disappear due to noise and errors in the initial data. The possibility of creating a “fake eddy” is provided so that the integrity of the track is not disturbed. A “fake eddy” is a copy of the last observed eddy (with a particular size, amplitude, etc.) moving along the last observed real trajectory at the same speed. It is marked with a special mark for further exclusion during subsequent processing.

Results and Discussion

The domain of the research is 64° – 76° N, 5° W– 20° E (Figure 1). A total number of 235,365 eddy-observations were detected for the period 1993–2017. Eddy tracking algorithm applied to the eddy observations identified 22090 ACEs and 23242 CEs in the LB. We exclude tracks of all eddies with a lifetime less than 35 days (99% eddies) to exclude the vortices associated with synoptic variability, as well as errors that could arise due to the small discreteness of satellite measurements in the study basin. Only 120 CEs and 210 ACEs are found to satisfy the above criteria. Table 1 demonstrates the spatially averaged parameters of the long-lived (> 35 days) mesoscale eddies in the LB.

For further analysis, we divide the domain of the LB into two regions. The first is the area of the LV bounded by 69° – 71° N, 1° – 5° E (area 1; see Figure 1). The second is the rest of the domain (area 2). Further, we divide all eddies into 4 Groups based on the location of their genera-

Table 2. Mesoscale Eddy Distribution (%) Into 4 Groups in the LB (Depending on the Places of Their Formation and Dissipation)

Group	Type of eddies	
	CEs (120 tracks)	ACEs (210 tracks)
1	14.3%	26.2%
2	73.3%	69.5%
3	9.2%	3.8%
4	3.3%	0.5%

tion and dissipation in the two regions (area 1 and area 2):

- Group 1: eddies born and dissipated in area 1; 72 eddies.
- Group 2: eddies born and dissipated in area 2; 234 eddies.
- Group 3: eddies born in area 2 and dissipated in area 1; 19 eddies.
- Group 4: eddies born in area 1 and dissipated in area 2; 5 eddies.

Group 2 eddies dominate (Table 2) the number of both long-lived CEs (73.3%) and ACEs (69.5%). This is expected since area 2 considerably exceeds area 1. Group 1 eddies holds second place with 14.3% CEs and 26.2% ACEs. Note that the number of long-lived ACEs exceeds the number of CEs in Group 1 and is attributed to the presence of the anticyclonic LV. However, CEs also exist in a sufficient amount, notably localized in vicinities of two geographical points with centers at 69.5°N, 4°E and 70°N, 2.5°E (not shown). Our greatest interest is in Group 3 which includes eddies propagating to the LV region (area 1) from outside (area 2). Mesoscale eddies of this group are formed mainly in the region of the Norwegian current and tend to cyclonic rotation [Gordeeva *et al.*, 2019; Zinchenko *et al.*, 2019]. It turned out that only 5% of the total long-lived mesoscale eddies in the LB (only 19 eddies out of 330: 11 of CEs and 8 of ACEs) can represent this type. Group 4 eddies represents only 1.5% of the total number of long-lived eddies in the LB. Figure 2 illustrates the box plots with whiskers for 4 Groups of eddies. The statistical characteristics of the CEs and ACEs are almost identical within their Groups except for lifetime, which is 1.5 times longer for ACEs than CEs. However, the

differences between the Groups are more significant (Figure 2). Figure 2 and Table 1 are used to choose typical long-lived eddies with middle characteristics from each Group.

Next, we apply a co-localization method based on the joint analysis of eddy trajectories of the long-lived eddies and their inferred three-dimensional structures. The essence of the co-localization method is as follows. If a GLORYS12V1 profile is located within an eddy detected by the automatic identification and tracking algorithm we define this profile (temperature and salinity) as “profile inside eddies” otherwise “profile outside eddies”. To determine three-dimensional eddy structures in the LB and inherent heat/salt transports, we select the longest-lived eddies from each Group and study ACEs and CEs separately. Using this approach, we choose 8 eddies (one representative ACE and CE for each of the 4 Groups) for further analysis. Figure 3 demonstrates tracks of chosen eddies belonging to different Groups. To estimate T/S anomalies, we use the GLORYS12V1 reanalysis and apply a Lagrangian framework at each point of the track. We provide formal statistical analysis of eddy characteristics without filtrations of outliers. Notice that the azimuthal speed exceeds significantly the moving speed (a requirement for trapping of eddies).

The next step is to calculate T/S volume anomalies for these 8 eddies, which is necessary to estimate their heat and salt transports. We use 25-year time series of temperature and salinity in the daily database of GLORYS12V1 to calculate anomalies at the specified points along the eddy-track, assuming that the 25-year duration provides the average climate characteristics calculating for each day (the background of T/S). Figure 4–Figure 7 demonstrate the vertical temperature and salinity anomalies as well as temporal variability of temperature anomalies inside CE and ACE in each of the four Groups. Figures show that T/S anomalies of CEs and ACEs significantly change during their lifetime (see Figure 4–Figure 7c, Figure 7f). Moreover, zonal cross-sections of temperature and salinity demonstrate that the centers of eddies obtained from altimetry often do not match to the centers in the cross-sections. It can be explained by two reasons. Firstly, the spatial resolution of altimetry data (0.25° grid) is not enough for good compliance. The daily time resolution of altimetry

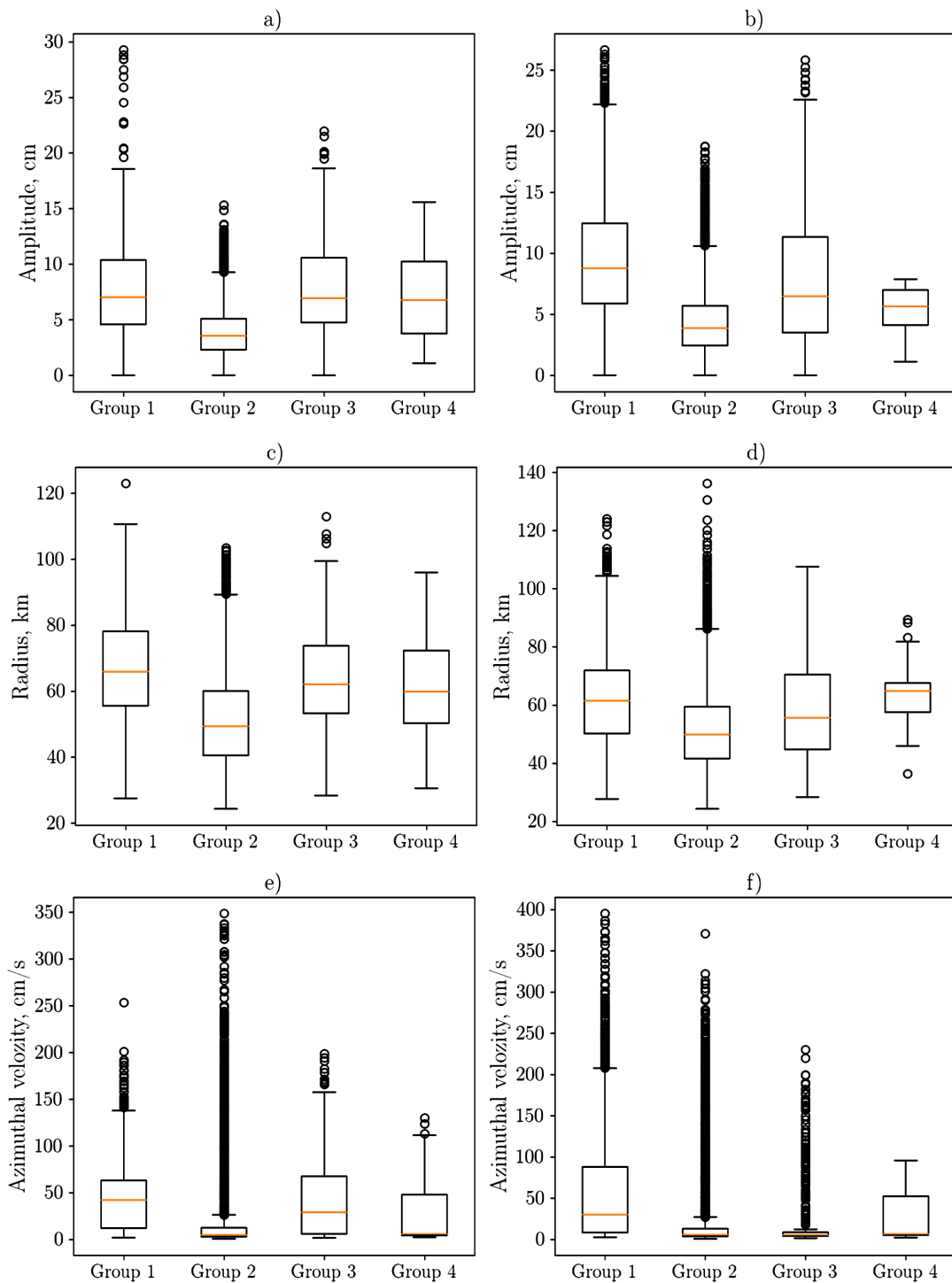


Figure 2. Box plot with whiskers for amplitude (cm), radius (km), azimuthal velocity (cm/s), moving speed along the tracks (km/day), a lifetime of CEs (on the left) and ACEs (on the right). The box sizes are 25–75% quantiles ($Q1 = 25\%$, $Q3 = 75\%$), the low ends of the whiskers are $Q1 - 1.5 \times (Q2 - Q1)$, the upper ends of the whiskers are $Q3 + 1.5 \times (Q2 - Q1)$, the yellow lines inside boxes indicate medians, the circles indicate outlier data.

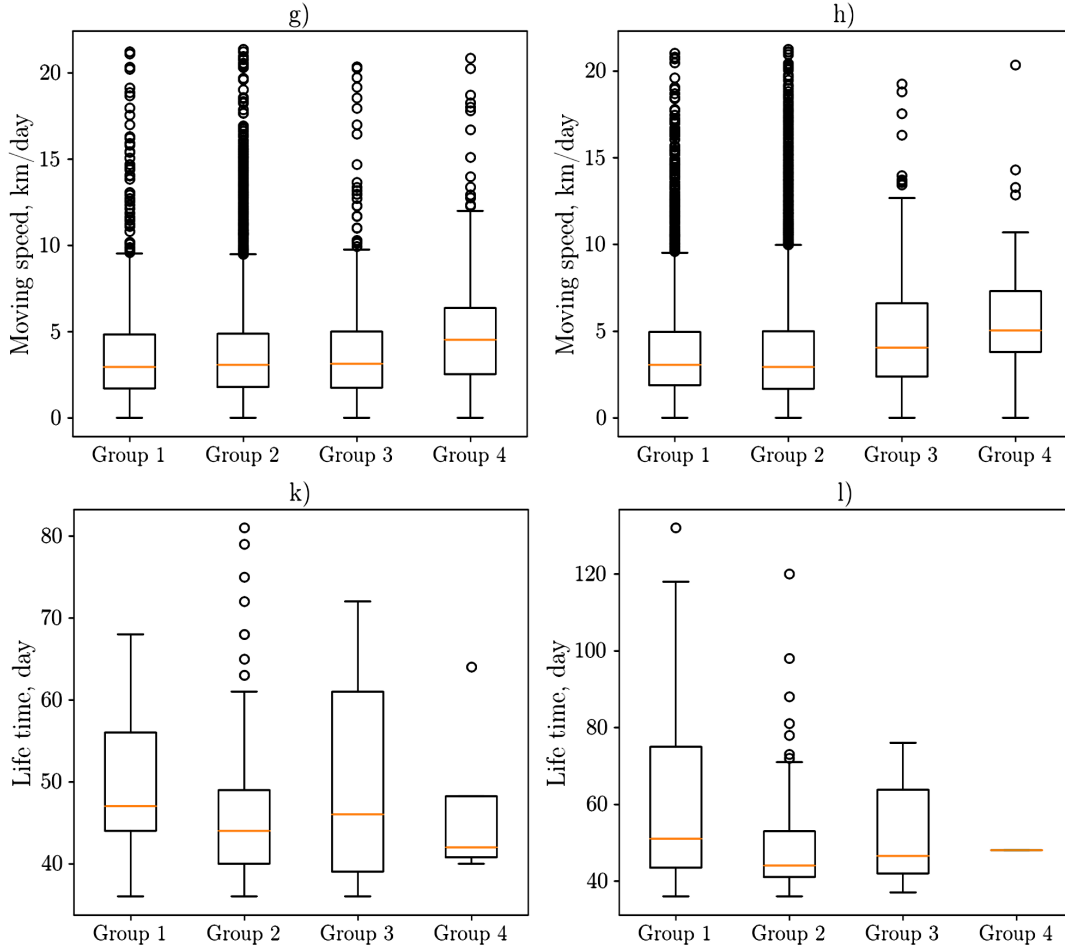


Figure 2. Continued.

try data (necessary for *Faghmous et al.* [2015] method) is obtained with usage optimal interpolation algorithm. Secondly, there is no precise compliance of coordinates of eddy centers with coordinates of relevant profiles. However, the maximum errors must be less the spatial resolution of GLO-RYS12V1 product. We realize that the approach based on analysis of the individual eddies from each Group allows us to obtain only averaged estimates of advection of heat and salt by mesoscale eddies for the LB. However, it can give a unique insight into the volume of T/S advection by eddies in the LB and shed light on the understanding of vortex dynamics in the basin.

We use temperatures cross-sections of 8 eddies (Figure 4–Figure 7a, Figure 7d) to determine the vortex border. Like meteorologists [Vorobiev, 1991], we defined eddy cores as areas within closed con-

tours and the eddy border is the most external closed contour. We use the assumption that eddies in the LB are formed more by temperature anomalies than by salinity [Bloshkina and Ivanov, 2016; Rossby et al., 2009a]. We thus now use the three-dimensional structure to estimate the relative eddy contribution to fluxes of volume, heat, and salt in the LB based on the knowledge of 3D-distributions of T/S anomalies in the eddies under consideration (see Figure 3). Following *Chaigneau et al.* [2011] and *Dong et al.* [2017], we calculated the available heat and salt content (AT and AS, respectively) for each of 4 Groups:

$$AT = \rho C_p \int T' dx dy dz$$

$$AS = \rho \int S' dx dy dz$$

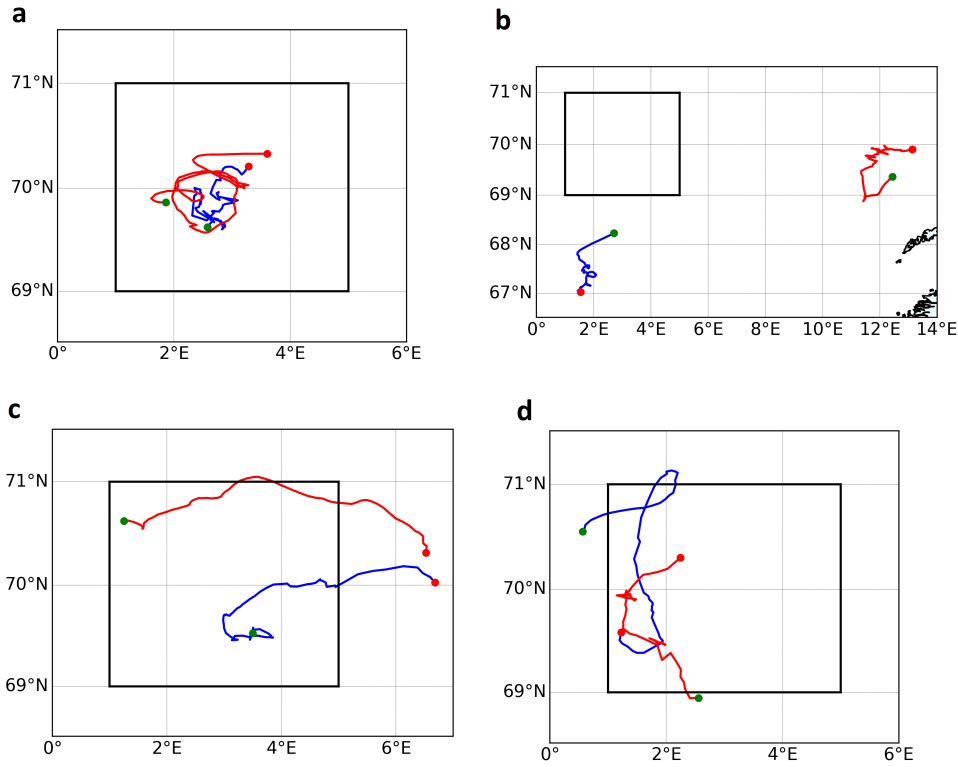


Figure 3. Tracks of analyzed long-lived eddies: (a) – Group 1, area 1, (b) – Group 2, area 2, (c) – Group 3, (d) – Group 4. The black rectangle shows the area of the Lofoten vortex (area 1). Blue lines display the cyclonic and red lines the anticyclonic eddies. The red points exhibit the location of the eddy generation, and the green points show the location of eddy dissipation.

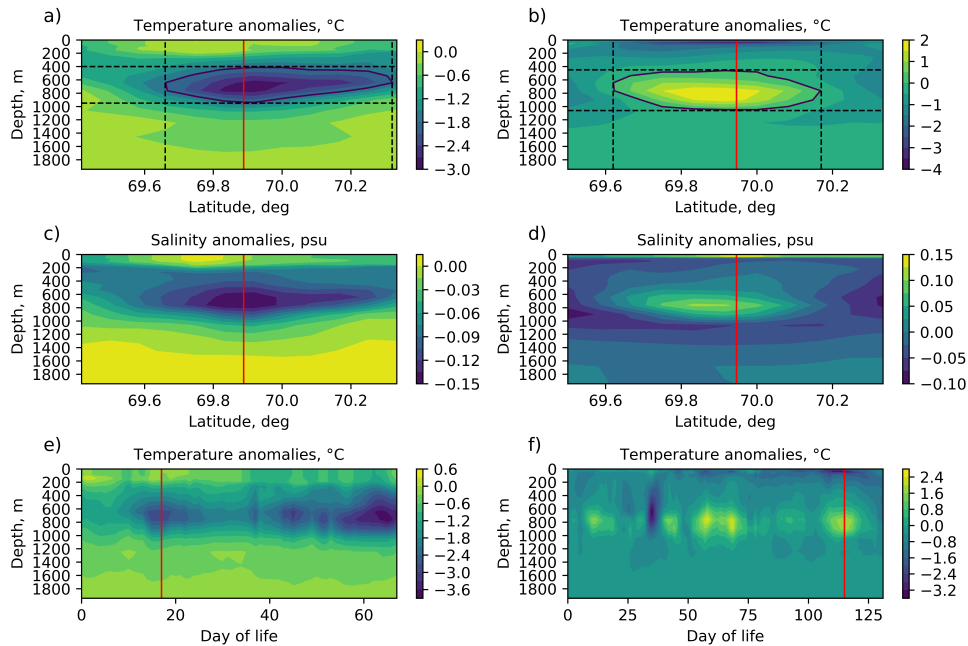


Figure 4. The cyclonic eddy (CE) (on the left) and the anticyclonic eddy (ACE) (on the right) for the Group 1: temperature anomalies (a), (d), salinity anomalies (b), (e), temporal variability of temperature anomalies for CE (c) and ACE (f). The red line shows the position of the eddy center according to altimetry data. Dashed lines indicate the eddy border.

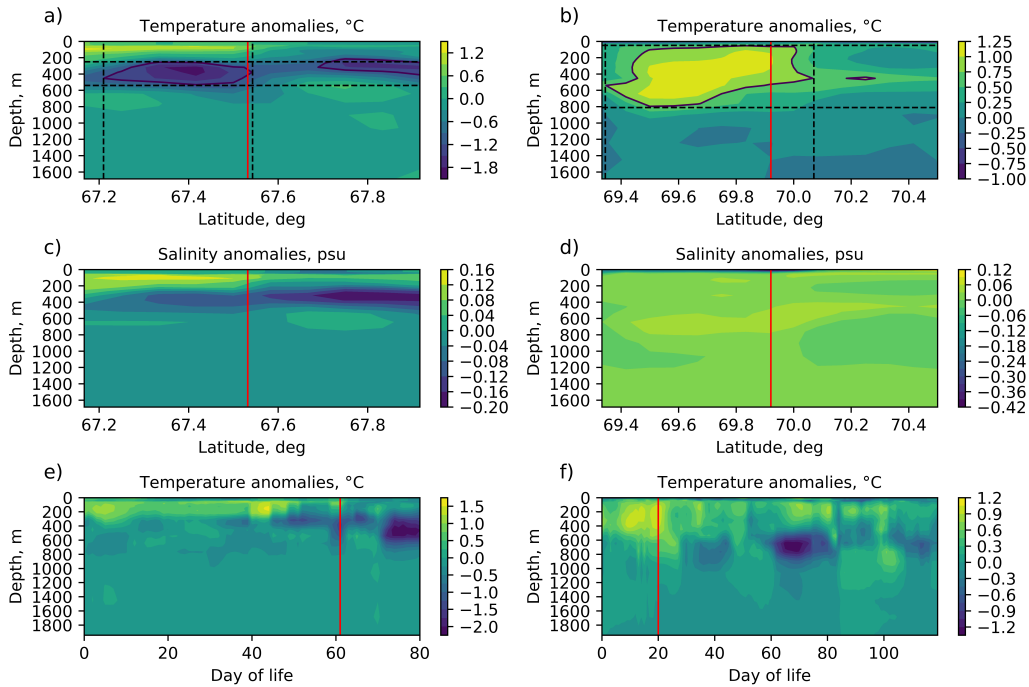


Figure 5. The cyclonic eddy (CE) (on the left) and the anticyclonic eddy (ACE) (on the right) for the Group 2: temperature anomalies (a), (d), salinity anomalies (b), (e), temporal variability of temperature anomalies for CE (c) and ACE (f). The red line shows the position of the eddy center according to altimetry data. Dashed lines indicate the eddy border.

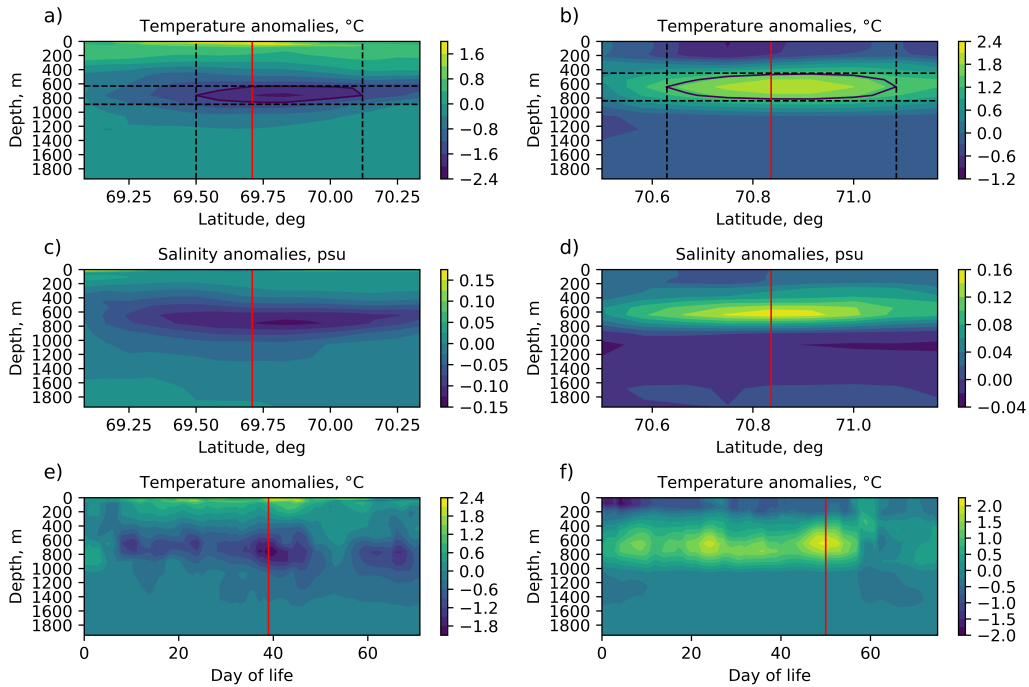


Figure 6. The cyclonic eddy (CE) (on the left) and the anticyclonic eddy (ACE) (on the right) for the Group 3: temperature anomalies (a), (d), salinity anomalies (b), (e), temporal variability of temperature anomalies for CE (c) and ACE (f). The red line shows the position of the eddy center according to altimetry data. Dashed lines indicate the eddy border.

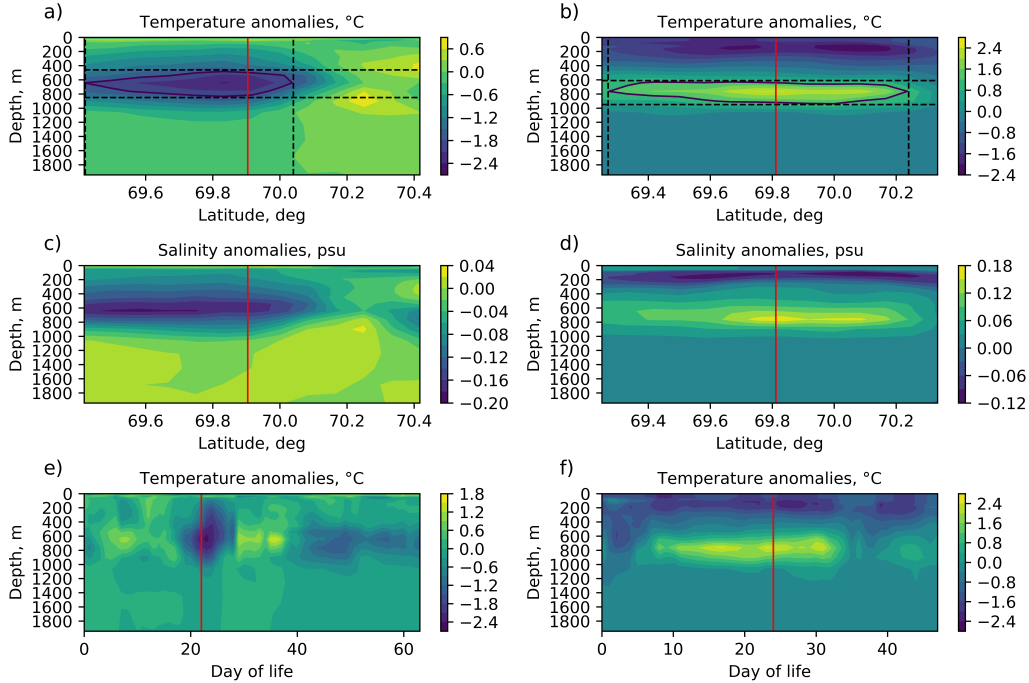


Figure 7. The cyclonic eddy (CE) (on the left) and the anticyclonic eddy (ACE) (on the right) for the Group 4: a latitudinal section of temperature anomalies (a), (d) and salinity anomalies (b), (e); temporal variability of temperature anomalies for CE (c) and ACE (f). The red line shows the position of the eddy center according to altimetry data. The red line notices the data of analysis. Dashed lines indicate the eddy border.

Here the respective mean upper ocean density and heat capacity are $\rho = 1025 \text{ kg m}^{-3}$ and $C_p = 4200 \text{ J kg}^{-1} \text{ }^\circ\text{C}^{-1}$. T' is the eddy-induced potential temperature anomaly, S' is the eddy-induced salinity anomaly. The results are detailed in Table 3. Note that in contrast to *Chaigneau et al.* [2011] and *Dong et al.* [2017] we calculate AT and AS in 3D-structures determined inside the last external closed surface of eddies. Figure 4–Figure 7 show vertical sections of these eddies where graphs “a” and “d” demonstrate the boundary limits of eddies. Figure 4–Figure 7 show that all considered eddies have a large thickness, and their horizontal sizes are very large, too. It is a reason why eddy volume and eddy volume transports are quite significant despite the small moving speed of these eddies.

Table 3 demonstrates different characteristics of eddies including heat and salt content: AT and AS, respectively. Note the values of AT and AS are positive for ACEs and negative for CE. High values of AT and AS for ACEs in Group 2 and 3 are not surprising because anticyclonic eddies generated at the periphery of the NwASC [see *Isachsen, 2015*]

keep the Atlantic Water heat and salt. Notably, the Group 4 ACEs have much higher AT and AS. This can be explained by the choice of the typical eddy from a small number of eddies (see Table 2). Also, it is important to note the high AT and AS values of Group 1 CE. These cyclonic eddies surrounding the quasi-permanent anticyclonic LV form a powerful ring of eddies like a shield [*Carton, 1992; Toth and Hazi, 2010*]. The absolute magnitude of AT of CE is 5.47 times greater in this region than AT of ACEs, and the coefficient is 7.0 for AS. This implies to the presence of a shield consisting of many cyclonic eddies around the LV which in turn is very important for the existence and stability of the vortex.

Following *Chaigneau et al.* [2011] and *Dong et al.* [2017], we also calculate heat and salt transports for different Groups of mesoscale eddies in the LB as well as total and annual values. Table 3 demonstrates that heat and salt transports by CE of Group 1 are much higher, than those by CE of other groups. Group 2 eddies comprise

Table 3. Thermohaline Contents and Associated Transports Integrated Over the Volume of the Long-Lived Cyclonic and Anticyclonic Eddies in the LB

Characteristics	Group 1		Group 2		Group 3		Group 4	
	CE	ACE	CE	ACE	CE	ACE	CE	ACE
Date of birth	1998-12-11	2000-10-02	2004-10-22	2015-07-30	2003-08-28	2001-12-31	2017-08-15	1993-11-18
Lifetime (days)	68	132	81	120	72	76	64	48
Thickness, m	550	600	300	760	260	410	300	340
Radius, km	36.63	30.52	18.59	39.96	34.41	29.14	26.92	53.83
Moving speed, m/s	0.03	0.03	0.03	0.01	0.01	0.01	0.03	0.06
Volume ($\times 10^{12}$, m ³)	2.32	1.61	0.33	1.50	0.97	0.69	0.68	2.73
Volume transport (Sv)	1.29	1.11	0.23	0.80	0.10	0.32	0.43	2.18
AT ($\times 10^{19}$, J)	-1.84	0.38	-0.15	1.23	-0.59	0.68	-0.6	1.76
AS ($\times 10^{11}$, kg)	-2.3	0.42	-0.18	0.87	-0.95	1.07	-1.02	2.87
Heat transport ($\times 10^{13}$, W)	-1.04	0.19	-0.12	0.27	-0.08	0.20	-0.37	1.3
Salt transport ($\times 10^5$, kg s ⁻¹)	-1.33	0.19	-0.14	0.19	-0.13	0.32	-0.68	2.05
Total heat transport ($\times 10^{13}$, W)	-17.68	10.45	-10.56	39.42	-0.88	1.6	-1.48	1.3
Total salt transport ($\times 10^5$, kg s ⁻¹)	-22.61	10.45	-12.32	27.74	-1.43	2.56	-2.72	2.05
Annual heat transport ($\times 10^{12}$, W)	-7.07	4.18	-4.22	15.76	-0.35	0.64	-0.59	0.52
Annual salt transport ($\times 10^4$, kg s ⁻¹)	-9.04	4.18	-4.93	11.10	-0.57	1.02	-1.09	0.82

more than 70% of the total long-lived eddies and hence it is not surprising that the total heat transport (39.42×10^{13} W) of Group 2 ACEs is much larger compared to rest. Similarly, total salt transport by ACEs is also maximum for Group 2 eddies (10.45×10^5 kg s⁻¹). On the other hand, total heat transport associated with CEs is maximum for Group 1 eddies (-17.68×10^{13} W) and is attributed to the large heat carried by individual eddies Group 1 CEs. Similarly, the total salt transport by CEs is observed to be maximum for Group 1 eddies (-22.61×10^5 kg s⁻¹). Next, we focus on the transport of heat and salt from the Norwegian Atlantic Current into the basin interior. Off the Lofoten Islands, where the continental slope is exceptionally steep, the NwASC becomes unstable and generates ACEs [Ikeda et al., 1989; Isachsen, 2015; Kohl, 2007] that drift towards the center of the basin along a cyclonic path [Raj et al., 2016; Volkov et al., 2013, 2015]. Thus, the LB eddies extract Atlantic waters from the NwASC and spread it all over the basin. The continuous supply of warm eddies leads to a general deepening

of isotherms in the LB, in particular in its deepest part, where the merging eddies form and maintain the LV [Belonenko et al., 2014; Ivanov and Korablev, 1995; Kohl, 2007; Raj et al., 2015; Soiland et al., 2016; Volkov et al., 2015]. Group 3, eddies generated in area 2 and dissipated in area 1, are responsible for this process. However, our analysis of mesoscale eddy activity based on satellite altimetry and method of automatic identification does not confirm significant heat and salt transport to the region of the Lofoten vortex location (area 1). Table 3 shows that heat and salt transport by Group 3 eddies drifting to the area 1 from outside (area 2) is not significant and is much less in comparison to the characteristic of eddies generated and dissipated directly in area 1 (Group 1 eddies). Nevertheless, volume transport is found to be higher for Group 3 ACEs (0.32 Sv) than for Group 3 CEs (0.10 Sv) although the volume of ACE (0.69×10^{12} m³) is less than the volume for CE (0.97×10^{12} m³). Similarly, heat and salt transports have greater magnitudes for ACEs than for CEs in Group 3. However, contrary to this, to

tal heat and salt transports are more for CEs than ACEs in Group 3 because the total number of CEs is more than ACEs (see Table 2). Table 3 also demonstrates that the impact of Group 3 CEs on the LV is more substantial in comparison to ACEs as annual heat and salt transports by Group 3 CEs are larger. We also determine total positive heat and salt transports to area 1 from outside by taking into account the negative values of CEs and the opposite contribution of eddies from Group 4. The magnitude of heat transport to the LV area from outside is 0.9×10^{13} W and salt transport is 1.8×10^5 kg s⁻¹. These values are for the whole period 1993–2017. Annual averages are 3.6×10^{11} W for the heat and 7.2×10^3 kg s⁻¹ for the salt. Since the associated volume transport in the basin needs to be zero, the difference in the values has to be covered by other mechanisms of advection and diffusion processes. Thus, these numbers assess cumulative transfers of heat and salt to area 1 from outside thereby influencing an annual winter regeneration of the Lofoten Vortex.

Summary

We use the automated identification and tracking method of *Faghmous et al.* [2015] to study the LB eddies. Focusing only on the long-lived mesoscale eddies (eddy life > 35 days), we found that the predominant type of both CEs (73.3%) and ACEs (69.5%) belong to Group 2 eddies, i.e. long-lived eddies, generated and disintegrated in area 2. While Group 1 eddies comes next (14.3%, CEs; 26.2%, ACEs), only 6% of all long-lived eddies are found to represent Group 3 (9.2%, CEs; 3.8%, ACEs), the Group, which includes eddies propagating to the LV neighborhood (area 1) from outside (area 2). The smallest is Group 4 (3.3%, CEs; 0.5%, ACEs), and it refers to eddies propagating in the opposite direction (from area 1 to area 2). Analysis of three-dimensional structures of the long-lived eddies in the LB and corresponding heat and salt transports is carried out using GLO-RYS12V1 reanalysis and by applying a Lagrangian framework at each point on every individual track. Available heat and salt content are estimated from the 3D T/S anomalies. Despite the small moving speed, the eddy volume transports are essential due

to the large size and horizontal scales of the eddies. There are significant values of AT and AS for cyclonic eddies in area 1, even though it is a region where anticyclonic eddies dominate. Cyclonic eddies in area 1 are found to surround the quasi-permanent anticyclonic LV to form a powerful ring of eddies like a shield.

The total heat transport is found to be maximum for Group 2 ACEs (39.42×10^{13} W), while heat transport associated with cyclonic eddies is comparatively lower (-10.56×10^{13} W). In comparison, the total heat transports by eddies of other groups are less. Notably, salt transport by Group 1 eddies is maximum and is associated with CEs (-22.61×10^7 kg s⁻¹). The salt transport by ACEs (10.45×10^7 kg s⁻¹) in Group 1 is less than that by CEs. The analysis does not confirm significant heat and salt transports to the area of the LV (area 1). Results show that heat and salt transports by eddies drifting to the area 1 from outside (Group 3 eddies) are not significant and much less in comparison to eddies born and dissipated in area 1 (Group 1 eddies). The volume transport of ACEs (0.32 Sv) in Group 3 is comparatively larger than that by CEs (0.10 Sv). However, contrary to this, total heat and salt transports are higher for CEs than ACEs in Group 3 because in the Group the total number of CEs is more than ACEs. The same is for annual heat and salt transports in Group 3 where the impact of cyclonic eddies on the LV is unexpectedly more substantial than anticyclonic eddies.

We assess heat and salt transports to area 1 from outside taking into account negative values of CEs and the opposite contribution of eddies from Group 4. The magnitude of heat transport is 0.9×10^{13} W and salt transport is 1.18×10^5 kg s⁻¹. Annual averages are 3.6×10^{11} W for the heat and 7.2×10^3 kg s⁻¹ for the salt. These numbers assess cumulative transfers of heat and salt to area 1 from outside thereby influencing an annual winter regeneration of the Lofoten Vortex. In summary, our study provides the first quantification of eddy induced heat and salt transport into the Lofoten Basin. Although the associated volume transport in the basin needs to be zero, the last means the advection of a heat or salt transports into an area of the Lofoten Vortex by mesoscale eddies has a positive balance. However, it concerns only the advection by eddies where the inflow exceeds the outflow. Therefore, the difference in the values has

to be covered by other mechanisms of advection and diffusion processes.

Acknowledgments. The authors acknowledge the support provided by the Russian Science Foundation (RSF, project No. 18-17-00027).

References

- Alexeev, G. V., M. V. Bagryantsev, et al. (1991), Structure and circulation of water masses in the area of an anticyclonic vortex in the north-eastern part of the Norwegian Sea, *Probl. Arctic Antarct.*, *65*, 14–23. (in Russian)
- Alexeev, V. A., V. V. Ivanov, et al. (2016), Convective structures in the Lofoten Basin based on satellite and Argo data, *Izv. Atmos. Ocean. Phys.*, *52*, No. 9, 1064–1077, [Crossref](#)
- Bashmachnikov, I. L., M. A. Sokolovskiy, et al. (2017), On the vertical structure and stability of the Lofoten vortex in the Norwegian Sea, *Deep-Sea Res. I*, *128*, 1–27, [Crossref](#)
- Belonenko, T. V., et al. (2018), Horizontal advection of temperature and salinity by Rossby waves in the North Pacific, *International Journal of Remote Sensing*, *39*, No. 8, 2177–2188, [Crossref](#)
- Belonenko, T. V., D. L. Volkov, et al. (2014), Circulation of waters in the Lofoten Basin of the Norwegian Sea, *Vestn. S. Petersburg Un-ta*, *7*, No. 2, 108–121. (in Russian)
- Belonenko, T. V., A. V. Koldunov, V. R. Foux (2011), Advecting Chlorophyll by Rossby Waves, *Vestn. S. Petersburg Un-ta*, *7*, No. 4, 106–109. (in Russian)
- Bjork, G., B. G. Gustafsson, A. Stigebrandt (2001), Upper layer circulation of the Nordic seas as inferred from the spatial distribution of heat and freshwater content, *Polar Res.*, *20*, 161–168, [Crossref](#)
- Bloshkina, E. V., V. V. Ivanov (2016), Convective structures in the Norwegian and Greenland Seas based on simulation results with high spatial resolution, *Proc. Hydromet. Research Center of the Russian Federation*, *361*, 146–168. (in Russian)
- Carton, X. J. (1992), On the Merger of Shielded Vortices, *EPL (Europhysics Letters)*, *18*, No. 8, [Crossref](#)
- Chaigneau, A., M. Le Texier, et al. (2011), Vertical structure of mesoscale eddies in the eastern South Pacific Ocean: A composite analysis from altimetry and Argo profiling floats, *J. Geophys. Res.*, *116*, C11025, [Crossref](#)
- Chelton, D. B., R. A. DeSzoeke, et al. (1998), Geographical variability of the first baroclinic Rossby radius of deformation, *J. Phys. Oceanogr.*, *28*, 433–460, [Crossref](#)
- Chelton, D. B., P. Gaube, et al. (2011), The influence of nonlinear mesoscale eddies on near-surface oceanic chlorophyll, *Science*, *334*, No. 6054, 328–332, [Crossref](#)
- Dong, C., J. C. McWilliams, et al. (2014), Global heat and salt transports by eddy movement, *Nature Communications*, *5*, 3294, [Crossref](#)
- Dong, D., P. Brandt, et al. (2017), Mesoscale eddies in the Northwestern Pacific Ocean: Three-dimensional eddy structures and heat/salt transports, *J. Geophys. Res.*, *122*, 9795–9813, [Crossref](#)
- Faghmous, J. H., I. Frenger, et al. (2015), A daily global mesoscale ocean eddy dataset from satellite altimetry, *Sci. Data*, *2*, 150028, [Crossref](#)
- Fedorov, A. M., I. L. Bashmachnikov, T. V. Belonenko (2019), Winter convection in the Lofoten Basin according to ARGO buoys and hydrodynamic modeling, *Vestn. S. Petersburg Un-ta, Earth Sciences*, *64*, No. 3, 491–511, (in Russian) [Crossref](#)
- Gaube, P., D. B. Chelton, et al. (2015), Satellite observations of mesoscale eddy-induced Ekman pumping, *J. Phys. Oceanogr.*, *45*, No. 1, 104–132, [Crossref](#)
- Gordeeva, S., V. Zinchenko, et al. (2019), Pattern of mesoscale eddy activity in the Lofoten Basin based on statistical analysis, *Advanced in Space Res.*, [Crossref](#)
- Ikeda, M., J. A. Johannessen, et al. (1989), A process study of mesoscale meanders and eddies in the Norwegian Coastal Current, *J. Phys. Oceanogr.*, *19*, 20–35, [Crossref](#)
- Ivanov, V. V., A. A. Korabely (1995), Dynamics of an intrapycnocline lens in the Norwegian Sea, *Russ. Meteorol. Hydrol.*, *10*, 55–62. (in Russian)
- Isachsen, P. E. (2015), Baroclinic instability and the mesoscale eddy field around the Lofoten Basin, *J. Geophys. Res.*, *120*, No. 4, 2884–2903, [Crossref](#)
- Jakobsen, P. K., M. H. Ribergaard, et al. (2003), Near-surface circulation in the northern North Atlantic as inferred from Lagrangian drifters: Variability from the mesoscale to interannual, *J. Geophys. Res.*, *108*, C8, [Crossref](#)
- Kohl, A. (2007), Generation and stability of a quasi-permanent vortex in the Lofoten Basin, *J. Phys. Oceanogr.*, *37*, 2637–2651, [Crossref](#)
- Koszalka, I., J. H. LaCasce, et al. (2011), Surface circulation in the Nordic seas from clustered drifters, *Deep-Sea Res. I*, *58*, 468–485, [Crossref](#)
- Kubryakov, A. A., T. V. Belonenko, S. V. Stanichny (2016), Impact of the mesoscale eddies on the sea surface temperature in the North Pacific Ocean, *Modern Problems of Remote Sensing of the Earth from Space*, *13*, No. 2, 124–133, (in Russian) [Crossref](#)
- Lozier, M. S. (1997), Evidence for large-scale eddy-driven gyres in the North Atlantic, *Science*, *277*, No. 5324, 361–364, [Crossref](#)
- Mork, K. A., O. Skagseth (2010), A quantitative description of the Norwegian Atlantic Current by combining altimetry and hydrography, *Ocean Science*, *6*, 901–911, [Crossref](#)
- Morrow, R., P. Y. Le Traon (2012), Recent advances in observing mesoscale ocean dynamics with

- satellite altimetry, *Advances in Space Res.*, 50, No. 8, 1062–1076, [Crossref](#)
- Morrow, R., R. Coleman, et al. (1994), Surface eddy momentum flux and velocity variances in the Southern Ocean from Geosat altimetry, *Journal of Physical Oceanography*, 24, No. 10, 2050–2071, [Crossref](#)
- Orvik, K. A. (2004), The deepening of the Atlantic water in the Lofoten Basin of the Norwegian Sea, demonstrated by using an active reduced gravity model, *Geophys. Res. Lett.*, 31, L01306, [Crossref](#)
- Poulain, P.-M., A. Warn-Varnas, P. P. Niiler (1996), Near-surface circulation of the Nordic seas as measured by Lagrangian drifters, *J. Geophys. Res.*, 101, No. C8, 18,237–18,258, [Crossref](#)
- Raj, R. P., L. Chafik, et al. (2015), The Lofoten Vortex of the Nordic Seas, *Deep-Sea Res. I*, 96, 1–14, [Crossref](#)
- Raj, R. P., J. A. Johannessen, et al. (2016), Quantifying mesoscale eddies in the Lofoten Basin, *J. Geophys. Res.*, 121, 4503–4521, [Crossref](#)
- Richards, C. G., F. Straneo (2015), Observations of Water Mass Transformation and Eddies in the Lofoten Basin of the Nordic Seas, *Journal of Phys. Oceanogr.*, 45, No. 6, [Crossref](#)
- Rosby, T., V. Ozhigin, et al. (2009a), An isopycnal view of the Nordic Seas hydrography with focus on properties of the Lofoten Basin, *Deep-Sea Res. I*, 56, No. 11, 1955–1971, [Crossref](#)
- Rosby, T., M. D. Prater, H. Soiland (2009b), Pathways of inflow and dispersion of warm waters in the Nordic seas, *J. Geophys. Res.*, 114, C04011, [Crossref](#)
- Skagseth, O., A. Slotte, et al. (2015), Characteristics of the Norwegian Coastal Current during Years with High Recruitment of Norwegian Spring Spawning Herring (*Clupea harengus* L.), *PLoS ONE*, 10, No. 12, e0144117, [Crossref](#)
- Soiland, H., T. Rossby (2013), On the structure of the Lofoten Basin Eddy, *J. Geophys. Res.*, 118, 4201–4212, [Crossref](#)
- Soiland, H., L. Chafik, T. Rossby (2016), On the long-term stability of the Lofoten Basin Eddy, *J. Geophys. Res.*, 121, 4438–4449, [Crossref](#)
- Toth, G., G. Hazi (2010), Merging of shielded Gaussian vortices and formation of a tripole at low Reynolds numbers, *Physics of Fluids*, 22, 053101, [Crossref](#)
- Volkov, D. L., L.-L. Fu (2008), The role of vorticity fluxes in the dynamics of the Zapiola Anticyclone, *J. Geophys. Res.*, 113, C11015, [Crossref](#)
- Volkov, D. L., T. V. Belonenko, V. R. Foux (2013), Puzzling over the dynamics of the Lofoten Basin – a sub-Arctic hot spot of ocean variability, *Geophys. Res. Lett.*, 40, No. 4, 738–743, [Crossref](#)
- Volkov, D. L., A. Kubryakov, R. Lumpkin (2015), Formation and variability of the Lofoten Basin vortex in a high-resolution ocean model, *Deep-Sea Res. I*, 105, 142–157, [Crossref](#)
- Vorobiev, V. I. (1991), *Synoptic Meteorology*, 612 pp. Hydrometeoizdat, Leningrad. (in Russian)
- Wunsch, C., P. Heimbach, et al. (2009), The global general circulation of the ocean estimated by the ECCO-consortium, *Oceanography*, 22, 88–103, [Crossref](#)
- Yu, L.-S., A. Bosse, et al. (2017), The Lofoten Basin eddy: Three years of evolution as observed by Seagliders, *J. Geophys. Res.*, 122, 6814–6834, [Crossref](#)
- Zinchenko, V. A., S. M. Gordeeva, et al. (2019), Analysis of Mesoscale eddies in the Lofoten Basin based on satellite altimetry, *Fundamentalnaya i Prikladnaya Gidrofizika*, 12, No. 3, 46–54, (in Russian) [Crossref](#)
- Zhmur, V. V. (2011), *Mesoscale Vortices of the Ocean*, 384 pp. GEOS, Moscow. (in Russian)

Corresponding author:

Tatyana Belonenko, Saint Petersburg State University, 7–9, Universitetskaya nab., 199034 Saint Petersburg, Russia. (btvlisab@yandex.ru)